Nuclear Science and Techniques (2026) 37:109
https://doi.org/10.1007/s41365-026-01944-z

Mechanisms of mirror energy difference for states exhibiting Thomas–Ehrman shift: Gamow shell model case studies of ^{18}Ne/^{18}O and ^{19}Na/^{19}O

Kun-Hao Li[1,2] · Pei-Yan Wang[2,3] · Jian-Guo Li[2,3,4] · Nicolas Michel[2,3] · Meng-Ran Xie[2,3] · Chun-Wang Ma[1,5] · Wei Zuo[2,3,4]

Received: 4 September 2025 / Revised: 22 October 2025 / Accepted: 11 November 2025 / Published online: 28 March 2026

Abstract
The mirror energy difference (MED) of the mirror state, particularly for states exhibiting the Thomas–Ehrman shift, serves as a sensitive probe of mirror symmetry breaking. We employ the Gamow shell model, which includes the inter-nucleon correlation and continuum coupling, to investigate the MED for *sd*-shell nuclei by taking ^{18}Ne/^{18}O and ^{19}Na/^{19}O as examples. Our GSM provides good descriptions of the excitation energies and MEDs for the ^{18}Ne/^{18}O and ^{19}Na/^{19}O. Furthermore, our calculations also reveal that the large MED of the mirror states is caused by the significant occupation of the weakly bound or unbound $s_{1/2}$ waves, giving the radial density distribution of the state in the proton-rich nucleus greater extension than that of mirror states in deeply bound neutron-rich nuclei. In addition, our GSM calculation shows that the contribution of the Coulomb interaction is different for the low-lying states in proton-rich nuclei, which significantly contributes to the MEDs of mirror states, as is well recognized. Finally, our GSM calculation indicates that the contributions of the nucleon–nucleon interaction are different for the mirror state, especially for the state of proton-rich nuclei bearing the Thomas–Ehrman shift, which also contributes to the significant mirror symmetry breaking with a large MED.

Keywords Mirror symmetry breaking · Thomas–Ehrman shift · Mirror energy difference · Continuum coupling · Gamow shell model

This work was supported the National Key R&D Program of China (Nos. 2024YFE0109800, 2024YFE0109802, and 2023YFA1606403), the National Natural Science Foundation of China (Nos. 12375123, 12205340, 12347106, and 12121005), the Natural Science Foundation of Henan Province (No. 242300421048), the Gansu Natural Science Foundation (Nos. 22JR5RA123 and 25JRRA467), and the State Key Laboratory of Nuclear Physics and Technology, Peking University (No. NPT2020KFY13). The numerical calculations in this paper have been done on Hefei advanced computing center.

✉ Jian-Guo Li
jianguo_li@impcas.ac.cn

✉ Nicolas Michel
nicolas.michel@impcas.ac.cn

✉ Chun-Wang Ma
machunwang@126.com

1 College of Physics, Center for Theoretical Physics, Henan Normal University, Xinxiang 453007, China

2 CAS Key Laboratory of High Precision Nuclear Spectroscopy, Institute of Modern Physics, Chinese Academy of Sciences, Lanzhou 730000, China

3 School of Nuclear Science and Technology, University of Chinese Academy of Sciences, Beijing 100049, China

4 Southern Center for Nuclear-Science Theory (SCNT), Institute of Modern Physics, Chinese Academy of Sciences, Huizhou 516000, China

5 Institute of Nuclear Science and Technology, Henan Academy of Sciences, Zhengzhou 450015, China

1 Introduction

Exotic nuclear structures in drip-line nuclei have become a subject of great interest in recent years, as they are characterized by unique properties that exhibit significant differences from those of stable nuclei [1–5]. One of the most significant phenomena observed in these systems is the

Thomas-Ehrman shift (TES) [6, 7]. This effect is most pronounced in nuclei close to the proton drip lines, where the balance between the strong force and the Coulomb force is delicate. States exhibiting TES effects are often weakly bound or unbound, which is characteristic of open quantum systems, while their neutron-rich mirror counterparts remain deeply bound, resulting in a large mirror energy difference (MED) in their isobaric states [6–11]. The large MEDs are attributed to their proximity to near-threshold effects, in which the continuum effects must be well treated. Consequently, a thorough comprehension of the Thomas-Ehrman shift is pivotal for elucidating the dynamics of weakly bound and unbound nuclear systems and understanding the mechanisms underlying mirror symmetry breaking in mirror nuclei.

Two possible reasons exist for the states with large MED: external or internal characteristics. If the extended single-particle wave functions of weakly bound or unbound *s*- or *p*-waves are significantly occupied in the considered states, the large MED is of an external nature, as in the TES states [9, 12, 13]. The second possibility is related to configuration mixing (see Refs. [14, 15]), is of internal nature. In this case, the extended wave function is given via strong configuration mixing, in which a few nodal states of *s* or *p* waves are included in the calculations. These two external and internal effects are different but can be intertwined in complex ways. For instance, the inversion of ground states in the ^{16}F and ^{16}N mirror nuclei is primarily due to the unbound proton $1s_{1/2}$ orbital, which can also be well described in GSM calculations within the configuration mixing framework [13, 16].

The *sd*-shell nuclei, situated at the boundary between the light and heavy nuclei, exhibit a wide range of nuclear structure phenomena that remain somewhat mysterious [17]. In recent years, these nuclei have been extensively studied using various experimental techniques [18–21]. A wealth of information on the Thomas-Ehrman shift has been gleaned from *sd*-shell proton drip-line nuclei, where numerous states exhibiting significant TES effects have been identified [8–10, 22]. For instance, the mirror pairs ^{18}Ne/^{18}O [8, 23] and ^{19}Na/^{19}O [22] serve as notable examples. For *sd*-shell nuclei, the TES is mainly driven by *s*-waves. Indeed, the proton $1s_{1/2}$ orbital is weakly bound or unbound in proton drip-line nuclei, whereas the neutron $1s_{1/2}$ orbital is well bound in their mirror neutron-rich nuclei.

Several theoretical models have been developed to probe the mirror asymmetry for mirror nuclei, such as the standard shell model (SM) [24–28], mean-field calculations [29, 30], and ab initio approaches [23, 31–34]. Within the standard SM calculations, weakly bound and unbound wave functions on eigenenergies are indirectly considered by phenomenologically adjusting the matrix element related to $1s_{1/2}$ orbit [9, 12]. Mean-field calculations, such as the Skyrme–Hartree–Fock, have also been extensively employed in MED studies [29, 30]. However, these models involve parameters constrained by data [24, 29, 35]. In recent years, ab initio approaches, such as the ab initio valence-space in-medium similarity renormalization group, have also been applied to study MEDs of *sd*-shell nuclei [10, 11, 23, 31–34, 36], in which the extended many-body wavefunctions are partially described using a large number of HO spaces. Moreover, current theoretical calculations have pointed out that the TES is caused by the repulsive Coulomb interaction and the occupations of weakly bound or unbound *s*- or *p*-waves for the valence protons. However, detailed studies on the TES mechanism are lacking. In recent shell model calculations [28], the TES was investigated using the calculated spectroscopic factors. Moreover, in our previous work [36], we compared the results of the MED calculated using the shell model with spectroscopic factors and the *ab initio* valence-space in-medium similarity renormalization ground approach. The two models yielded similar results.

One of the major challenges in studying drip-line nuclei is accounting for the interplay between configuration mixing and continuum effects. The Gamow shell model (GSM) [14, 15, 23, 31, 37–42] has emerged as a powerful tool in this regard, as it provides a unified framework for describing the structure of nuclei close to the particle emission threshold and allows for an accurate understanding of the exotic properties of drip-line nuclei. Based on the above situation, we employ the GSM to investigate the significant mirror symmetry breaking with large MED values and the mechanism behind it for the *sd*-shell nuclei, taking the ^{18}Ne/^{18}O and ^{19}Na/^{19}O mirror partners as examples.

2 Method

The GSM is a multiconfiguration shell model framework that works in the picture of a core plus valence nucleons [39, 40, 43–45]. At the heart of the GSM lies the utilization of the one-body Berggren basis [46], which possesses bound, resonance, and scattering states generated by a finite-range potential, typically of Woods–Saxon (WS) type (see details in Ref. [39, 40, 46]). The GSM Hamiltonian matrix is characterized by complex symmetry [39, 40]. The overlap method, along with the Jacobi–Davidson method extended to complex-symmetric matrices, was adopted to diagonalize and identify many-body resonance eigenstates [39, 40, 47]. Consequently, the GSM calculation includes both the inter-nucleon correlations and continuum coupling [39, 40, 43].

The many-body Schrödinger equation of the GSM Hamiltonian can be solved within the so-called cluster orbital shell model (COSM) formalism [48] (see Refs. [40, 49, 50]). The GSM Hamiltonian in COSM coordinates reads [40, 49, 50]:

$$\hat{H}_{\rm GSM}=\sum_{i=1}^{A_{\rm val}}\left(\frac{\mathbf{p}_i^2}{2\mu_i}+\hat{U}_i^{(\rm c)}\right)+\sum_{i<j}^{A_{\rm val}}\left(\hat{V}_{ij}+\frac{\mathbf{p}_i\cdot\mathbf{p}_j}{M_{\rm c}}\right), \quad (1)$$

where $A_{\rm val}$ is the number of valence nucleons, μ_i is the effective mass of the nucleon, $\hat{U}_i^{(\rm c)}$ is represented by a one-body WS potential mimicking the inert core. $\hat{V}_{ij}$ is the residual inter-nucleon interaction, which is modeled by a pionless effective field theory (EFT) interaction [51, 52], in which only two-body contact terms up to next-to-next leading order are considered. The regularization approach adopted in Refs. [44, 53–56] is used. The last term embodies the recoil effects induced by the finite mass of the core $M_{\rm c}$. The EFT interaction was optimized to reproduce the low-lying states of the selected nuclei.

In the present work, the ^{18}Ne/^{18}O and ^{19}Na/^{19}O mirror partners are considered as examples. The doubly magic nucleus ^{16}O was chosen as the inert core, and the $s_{1/2}$, $p_{1/2,3/2}$ and $d_{3/2,5/2}$ partial waves were represented by the Berggren basis, in which 40 discretization points were used in total for continuum states in each partial wave. The $f_{5/2,7/2}$ partial waves were treated using the HO basis, in which six HO states were adopted for each of the partial waves. To estimate the effects of higher orbitals, we compared the results after adding the $g_{7/2,9/2}$ partial waves under the HO basis. The difference in the binding and excitation energies of the states studied in the present work was less than 5 keV. Thus, higher partial waves are neglected. Only the Coulomb force is considered for the isospin non-conserving part of the GSM Hamiltonian. The contribution of the isospin-dependent part of the nuclear interaction to the TES is small, which is neglected in the present GSM calculations. The Hamiltonian used in Ref. [57] was adopted in this study. The calculated excitation energies of ^{18}Ne/^{18}O and ^{19}Na/^{19}O mirror partners are presented in Tables 1 and 2, which show good agreements with experimental data [58]. In the following section, the mechanisms of the mirror energies differences for the ^{18}Ne/^{18}O and ^{19}Na/^{19}O mirror partners are investigated in detail.

3 Results

Our GSM calculations accurately describe the excitation energies of the low-lying states for the mirror partners ^{18}Ne/^{18}O and ^{19}Na/^{19}O. To delve deeper into the significant mirror symmetry breaking observed in these mirror nuclei, we define the MED for a given state J^π as MED(J^π) $= E_x(T_z^<, J^\pi) - E_x(T_z^>, J^\pi)$, where $T_z^<$ and $T_z^>$ denote the negative and positive isospin projections $T_z = (N-Z)/2$, respectively, for a mirror pair. We have calculated MED values for mirror states in ^{18}Ne/^{18}O and ^{19}Na/^{19}O, as presented in Tables 1 and 2, along with experimental data. It is observed that in most states, the GSM-calculated MED values for low-lying states in the mirror partners ^{18}Ne/^{18}O and ^{19}Na/^{19}O align with the experimental data. Although the numerical differences in the excitation energies between the calculated and experimental values for some states are relatively large, they still exhibit the expected qualitative trend of MED. Meanwhile, the SM results are poor, demonstrating that coupling to continuum states plays an essential role in the study of mirror states bearing significant mirror symmetry breaking. However, an exception is noted for the 0_2^+ state in the ^{18}Ne/^{18}O mirror nuclei, where our GSM calculations yield larger values than those of the experimental data. Both our GSM calculations and the experimental data highlight significant mirror symmetry breaking in the 3_1^+ state of the

Table 1 Calculated excitation energies of ^{18}Ne/^{18}O with GSM and SM calculations in harmonic oscillator single *sd*− shell model space without including higher orbitals, along with experimental data [58]. The unit of excitation energy is given in MeV, and the units of particle decay width and MED are given in keV

J^π	^{18}Ne					^{18}O			MED		
	$E_{\rm exp}$	$E_{\rm GSM}$	$E_{\rm SM}$	$\Gamma_{\rm exp}$	$\Gamma_{\rm GSM}$	$E_{\rm exp}$	$E_{\rm GSM}$	$E_{\rm SM}$	EXP	GSM	SM
0_1^+	0	0	0		0	0	0	0	0	0	0
2_1^+	1.89	1.83	1.72		0	1.98	1.93	1.77	−95	−106	−50
4_1^+	3.38	2.72	2.08		0	3.56	2.72	2.21	−179	−3	−130
2_2^+	3.62	3.98	4.93		0	3.92	4.40	4.93	−304	−420	0
0_2^+	3.58	4.58	7.45		0	3.63	5.42	7.21	−58	−834	24
3_1^+	4.56	4.63	6.93	18	80	5.38	5.53	6.91	−817	−892	20

Table 2 Similar to Table 1, but for ^{19}Na/^{19}O

J^π	^{19}Na			^{19}O			MED		
	$E_{\rm exp}$	$E_{\rm GSM}$	$E_{\rm SM}$	$E_{\rm exp}$	$E_{\rm GSM}$	$E_{\rm SM}$	EXP	GSM	SM
$5/2_1^+$	0	0	0	0	0	0	0	0	0
$3/2_1^+$	0.12	0.64	0.83	0.10	0.71	0.81	24	−64	20
$1/2_1^+$	0.75	0.69	3.08	1.47	1.30	2.88	−727	−607	200

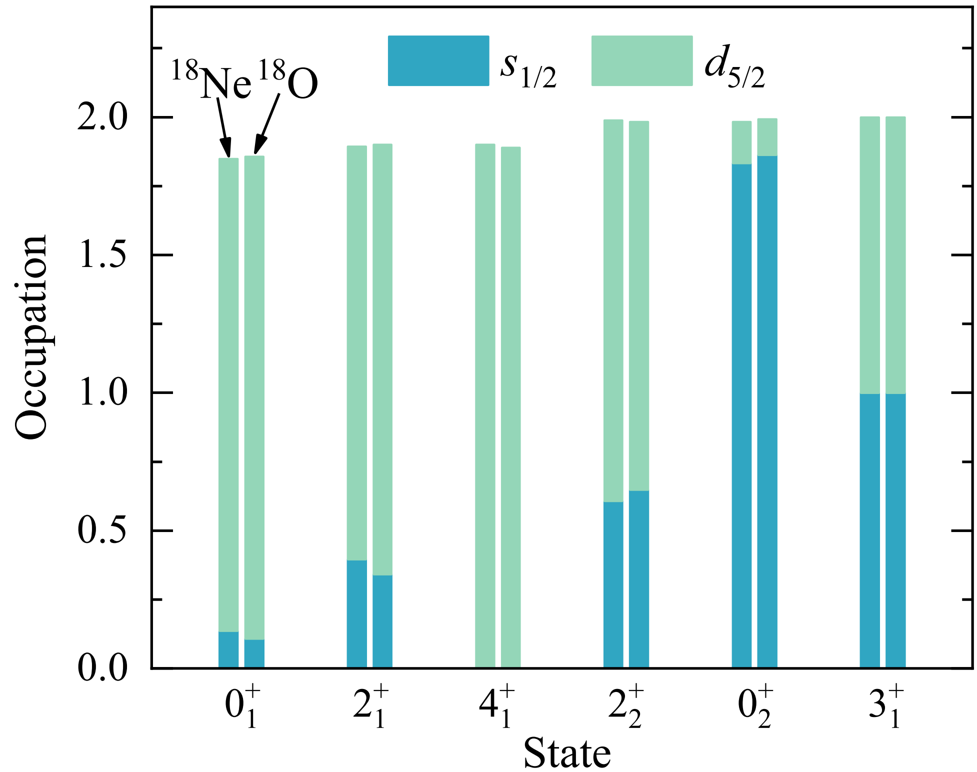

Fig. 1 (Color online) Average occupation numbers for the $s_{1/2}$ and $d_{5/2}$ partial waves in the low-lying states of the ^{18}Ne/^{18}O mirror pair, calculated using the GSM above the ^{16}O core

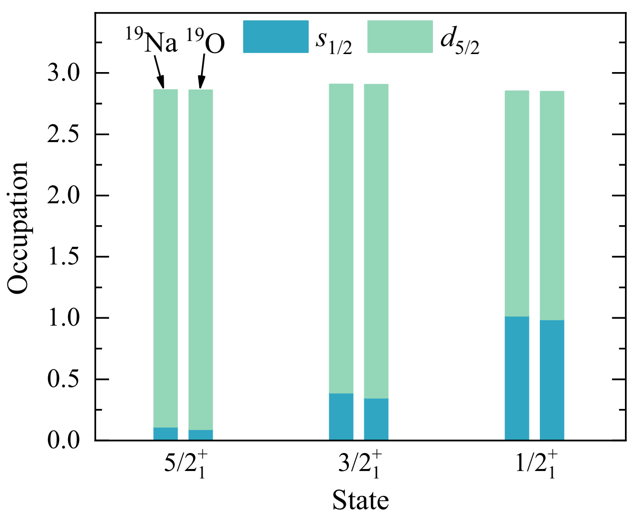

Fig. 2 (Color online) Similar to Fig. 1, but for low-lying states in ^{19}Na/^{19}O

^{18}Ne/^{18}O mirror nuclei and the $1/2_1^+$ state of the ^{19}Na/^{19}O mirror nuclei, as evidenced by their large MED values.

To investigate the significant mirror symmetry breaking and the associated large MEDs, we began by calculating the average occupations of the low-lying states through the GSM. The focus is particularly on the $s_{1/2}$ and $d_{5/2}$ partial waves above the ^{16}O core for the ^{18}Ne/^{18}O and ^{19}Na/^{19}O mirror nuclei, as shown in Figs. 1 and 2. Notably, other partial waves such as $d_{3/2}$ and $f_{5/2,7/2}$ exhibit negligible occupations and are, therefore, excluded from these figures. The calculated average occupations reveal almost identical patterns for the mirror states within the ^{18}Ne/^{18}O and ^{19}Na/^{19}O pairs. Our GSM calculations further indicate that states exhibiting significant mirror symmetry breaking with large MED values also show significant occupancy in the $s_{1/2}$ partial waves, which are markedly higher than in their respective ground states. For instance, the occupations of the $s_{1/2}$ partial wave for the 3_1^+ and $1/2_1^+$ states in the ^{18}Ne/^{18}O and ^{19}Na/^{19}O mirror pairs, respectively, are substantially greater than those of their ground states. Additionally, our calculations show that the 0_2^+ of ^{18}Ne/^{18}O demonstrates notable $s_{1/2}$ partial wave occupations compared to the ground states, resulting in a large MED. In contrast, experimental data provide a smaller MED value, hinting at a complex structure of the 0_2^+ states in ^{18}Ne/^{18}O that might not be fully captured by ^{16}O plus valence particle picture.

Aligned with results from other theoretical frameworks, such as the standard shell model and the ab initio VS-IMSRG approach, our results indicate that the significant mirror symmetry breaking with large MEDs observed in mirror states stems primarily from the extensive occupation of the $s_{1/2}$ partial waves, which are weakly bound or unbound in the proton-rich nucleus but deeply bound in

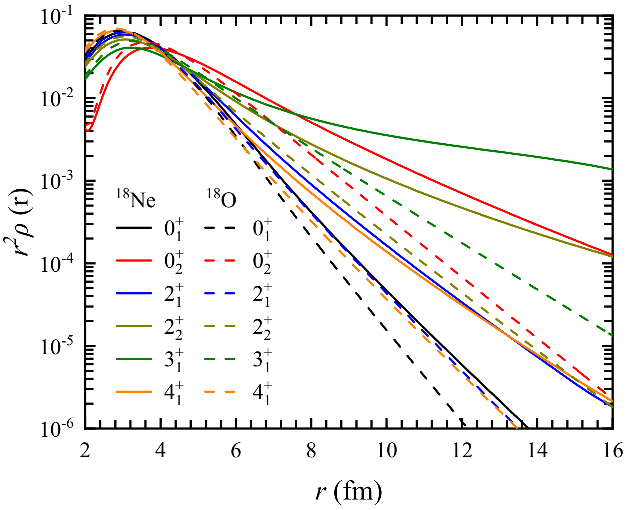

Fig. 3 (Color online) Calculated radial density distribution of valence protons and valence neutrons for low-lying mirror states in ^{18}Ne/^{18}O, respectively, above ^{16}O inner core, using GSM

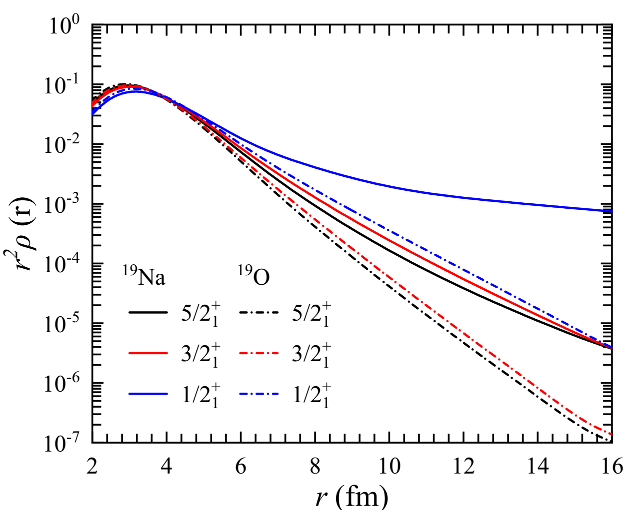

Fig. 4 (Color online) Similar to Fig. 3, but for low-lying states in ^{19}Na/^{19}O

its mirror neutron-rich nucleus, called TES. However, a deeper understanding of the mirror state bearing significant mirror symmetry breaking and a large MED value is lacking. The GSM is a suitable model that properly treats both the inter-nucleon correlations and continuum coupling to describe the properties of drip-line nuclei, including a precise description of the many-body wave function in the asymptotic regions [44, 57, 59, 60].

To elucidate the underlying mechanism of large MEDs, we conducted a detailed analysis of the radial density distributions of mirror states in ^{18}Ne/^{18}O and ^{19}Na/^{19}O pairs using the GSM. The results allow us to systematically compare the radial distributions of valence protons in proton-rich nuclei and those of valence neutrons in their neutron-rich mirror counterparts. The results are shown in Figs. 3 and 4 for ^{18}Ne/^{18}O and ^{19}Na/^{19}O mirror partners, respectively. Our GSM results reveal that the states characterized by minor mirror symmetry breaking with small MEDs exhibit almost identical radial density distributions, which decline sharply in the asymptotic regions, such as the ground states of both ^{18}Ne/^{18}O and ^{19}Na/^{19}O. This phenomenon is largely attributed to the dominance of $d_{5/2}$ partial waves, which are constrained within the nuclear region by high centrifugal and Coulomb barriers, despite the state being unbound. Conversely, GSM calculations depict the radial density distributions of the 3_1^+ state of ^{18}Ne and the $1/2_1^+$ state of ^{19}Na as more extended in the asymptotic region than their neutron-rich counterparts ^{18}O and ^{19}O, respectively. This disparity stems from the non-existent centrifugal barrier for the $s_{1/2}$ partial wave, leading to a more pronounced distribution in the proton-rich nucleus owing to the weakly bound or unbound nature of the $s_{1/2}$ partial wave. A similar mechanism underlies the formation of halo nuclei, where the valence nucleons occupy weakly bound s- or p- partial waves, resulting in an extended density distribution owing to the minimal or absent centrifugal barrier [14, 49, 61] . In previous works, these exotic phenomena that result from the mechanism for the extension of the $s-$ partial wave have been widely recognized. However, in reality, most theoretical models cannot directly provide the properties of this extension and its impact on physical phenomena when performing calculations, such as the results of our SM calculations within the single *sd* shell model space in Table 1, where the MEDs of all states for ^{18}Ne/^{18}O are quite small.

However, mirror symmetry breaking can be calculated using the traditional SM by introducing further approximations and modifications. For example, traditional SM calculations using the USDC interaction give the MED of the mirror $1/2_1^+$ state of ^{19}Na/^{19}O as −225 keV, which is significantly smaller than the experimental data of −727 keV. Moreover, the MED of the mirror $1/2_1^+$ state of ^{19}Na/^{19}O is mainly caused by the difference in the optimized single-particle energy for valence protons and neutrons in the USDC interaction [28]. Nevertheless, since the calculated MED is significantly smaller than the experimental data, they simulated the TES arising from continuum coupling through $\text{TES}_{\text{total}} \sim C^2S_{s_{1/2}}\text{TES}_{\text{sp}}$, where the $C^2S_{s1/2}$ is spectroscopic factors of proton $s_{1/2}$ orbital and TES_{sp} is single-particle TES [28]. The approximate treatment of the TES provides the MED value of the mirror states close to the experimental data. Based on this, the relationship between

TES and the extended $s_{1/2}$ partial wave in the mirror partner was determined indirectly. However, SM calculations cannot provide a direct description of the TES. Moreover, phenomenological adjustments to the matrix elements related to the proton $s_{1/2}$ orbital have also been employed in the SM to describe the indirect effects of weakly bound and unbound wave functions on eigenenergies. For $A \approx 20$ nuclei, the strength of the effective SM interactions involving the loosely bound proton $s_{1/2}$ orbit is significantly reduced in comparison with their mirror nuclei to calculate the significant mirror symmetry [12], in which the reduction factors of the two-body matrix elements related to the proton $s_{1/2}$ orbital are evaluated using the Woods–Saxon potential. The large MEDs in ^{18}Ne/^{18}O and ^{19}Na/^{19}O are well reproduced.

Unlike the SM calculation introduced above with the aforementioned corrections, our GSM calculations provide a more self-consistent direct calculation of the radial density distribution, yielding the expected MEDs without relying on other corrections and modifications. Moreover, our calculations directly reveal that the mirror states demonstrating significant mirror symmetry breaking with large MEDs possess many-body wave functions in proton-rich nuclei that are more extended than those in their neutron-rich mirror states, which further helps us understand the role of mirror symmetry breaking in shaping their properties.

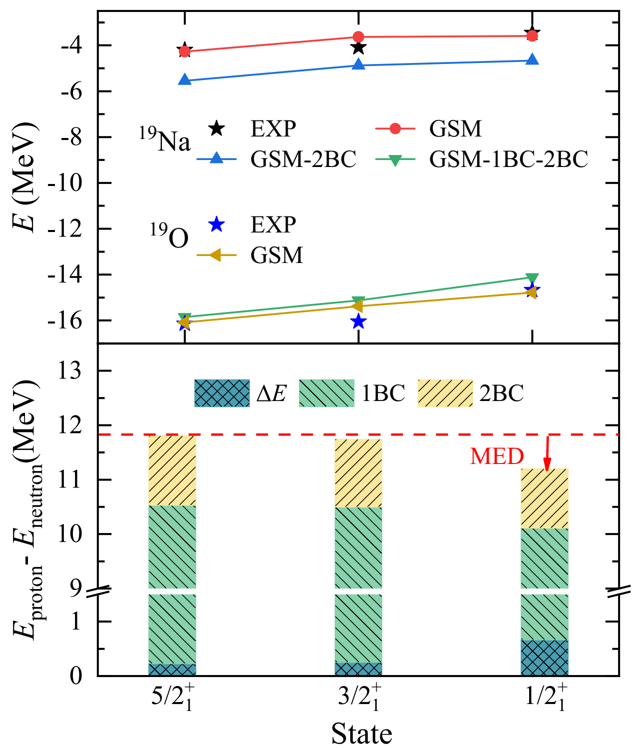

Fig. 6 (Color online) Similar to Fig. 5, but for low-lying states in ^{19}Na/^{19}O

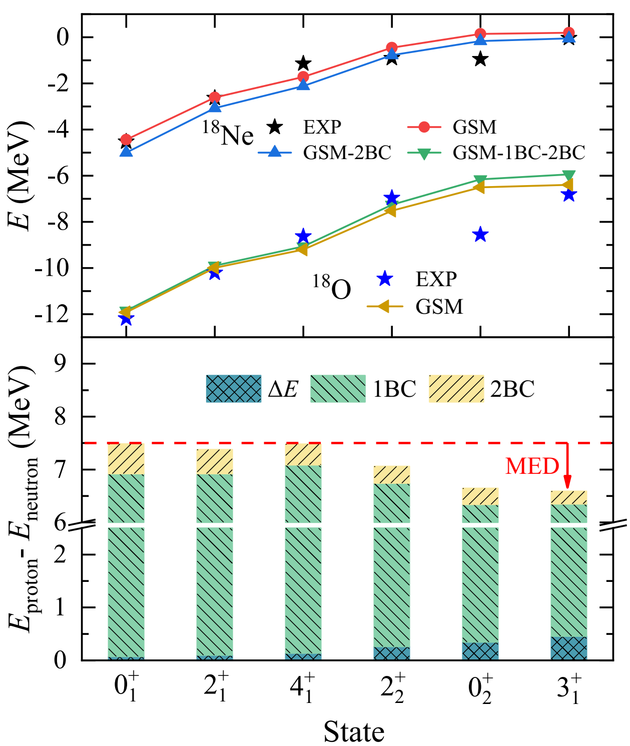

Fig. 5 (Color online) Upper panel: calculated energies (GSM), energies minus the two-body Coulomb contribution (GSM-2BC), and energies minus one- and two-body Coulomb total contributions (GSM-1BC-2BC) of low-lying states of ^{18}Ne using GSM, along with the energies of mirror states in ^{18}O, with respect to the ^{16}O inner core. The GSM results are also compared with the experimental data. Lower panel: the contribution for the calculated energy difference between the mirror states

The GSM Hamiltonian, as shown in Eq. (1) can be divided into nuclear interactions (encompassing core-nucleons and nucleon-–nucleon interactions) and Coulomb interactions (including one-body Coulomb (1BC) interactions between the inner core and valence protons and two-body Coulomb (2BC) interactions between valence protons). We performed further calculations to dissect the contributions from different parts of the Hamiltonian, aiming to shed light on the underlying mechanisms in mirror states exhibiting significant mirror symmetry breaking with a large MED.

The computed energies for the low-lying mirror states in the pairs ^{18}Ne/^{18}O and ^{19}Na/^{19}O, along with the experimental data [58], are shown in Figs. 5 and 6, respectively. To gain deeper insights, we also present the energy minus 2BC contribution (GSM-2BC) and energy minus 1BC and 2BC contributions (GSM-1BC-2BC) in proton-rich nuclei ^{18}Ne and ^{19}Na. Indeed, GSM-1BC-2BC also corresponds to the contribution of nuclear interactions. Within the isospin symmetry picture, the difference in mirror state energies should solely stem from Coulomb interactions, implying that the GSM-1BC-2BC values for a state in a proton-rich nucleus are the same as those for its mirror state in a neutron-rich nucleus.

Our GSM calculation shows that the GSM-1BC-2BC values for the ground states of ^{18}Ne and ^{19}Na closely align with the computed ground-state energies of their neutron-rich counterparts, ^{18}O and ^{19}O, respectively. The results indicate the preservation of mirror symmetry in these ground states. Conversely, for the excited 3_1^+ state in ^{18}Ne/^{18}O and the $1/2_1^+$ state in ^{19}Na/^{19}O, our GSM calculations showcase a deviation from this symmetry. To quantitatively examine this discrepancy, we introduced ΔE as the differential metric for significant mirror symmetry breaking. ΔE encapsulates the disparity between the GSM-1BC-2BC values in the state of the proton-rich nucleus and the energy calculated for the corresponding state in the neutron-rich mirror nucleus, which read as $\Delta E = \langle\Psi_{\text{proton}}|H_{NN}|\Psi_{\text{proton}}\rangle - \langle\Psi_{\text{neutron}}|H_{NN}|\Psi_{\text{neutron}}\rangle$. Here, Ψ_{proton} and Ψ_{neutron} correspond to the many-body wave functions of proton-rich and neutron-rich nuclei, respectively. The ΔE corresponds to the difference in the contribution of the nuclear interactions in the mirror state.

Our GSM calculations show that both ΔE and Coulomb interactions, including 1BC and 2BC, significantly influence the energy discrepancies observed in the mirror states. Predominantly, Coulomb interactions emerged as the dominant factor contributing to these differences. This is illustrated in the lower panels of Figs. 5 and 6, we detail the ΔE, 1BC, and 2BC contributions to the energy differences in the low-lying mirror states of ^{18}Ne/^{18}O and ^{19}Na/^{19}O mirror pairs. Our GSM results indicate that the energy differences in the ground states of ^{18}Ne/^{18}O primarily stem from Coulomb interactions, with ΔE contributing minimally. Furthermore, for ^{19}Na/^{19}O, the ΔE contribution was approximately 100 keV. Interestingly, we find varying contributions of ΔE, 1BC, and 2BC across different mirror states within each state. For instance, the 3_1^+ states in ^{18}Ne/^{18}O exhibit a higher ΔE contribution and lower Coulomb interactions relative to their ground states. The heightened ΔE values underscore the distinct contributions of nuclear interactions to mirror symmetry breaking in these systems, showcasing the complex interplay of forces that shape the energy landscapes of mirror nuclei.

In evaluating the MED, the ground-state energy of the mirror nuclei serves as the baseline, with the MED being determined by the discrepancy in the excitation energies of the corresponding mirror states. The energy difference of the ground states of the mirror nuclei was adopted as a reference, as illustrated by the red dashed lines in Figs. 5 and 6. The difference between the values of the ground and excited mirror states corresponds to the MED, highlighted by red arrows in these figures. The results revealed that both the ΔE values and Coulomb interaction exhibited significant variations across different mirror states, both contributing to the MED.

Furthermore, to validate our conclusion, we performed Gamow shell model calculations using an optimized Hamiltonian fitted to reproduce a series of selected experimental data for *sd* shell nuclei. Moreover, the optimized Hamiltonian has been employed to investigate the low-lying states in ^{21}Al [62] and ^{22}Si [63], as well as isospin symmetry breaking in these nuclei. Although the calculated excitation energies exhibited slight differences, the MED results aligned with both the current GSM calculations and the established conclusions regarding the MED mechanism.

4 Summary

Based on the GSM calculations, in which both the inter-nucleon correlation and continuum coupling are properly treated, we deduce that significant mirror symmetry breaking in mirror states, leading to large MED values, arises from the occupation of weakly bound or unbound $s_{1/2}$ partial waves in the proton-rich nucleus, while its counterpart in the neutron-rich nucleus remains deeply bound. This dichotomy culminates in a more expansive radial density distribution for states within the proton-rich nucleus than for their mirror counterparts. Additionally, the difference in the radial density distributions between the mirror states implies disparate contributions from nuclear interactions, underscored by significant ΔE values, which further highlights the presence of mirror symmetry breaking. Moreover, states with an extended radial density distribution tend to yield smaller Coulomb contributions than ground states characterized by more localized distributions. This factor chiefly accounts for the reduced excitation energies in states influenced by the Thomas-Ehrman shift effect, thereby engendering substantial negative MED values in mirror states. Our GSM calculations corroborate that both nuclear and Coulomb interactions play crucial roles in manifesting the significant mirror symmetry breaking associated with significant MED values.

Author contributions All authors contributed to the study conception and design. Material preparation, data collection and analysis were performed by Kun-Hao Li, Jian-Guo Li, Nicolas-Michel and Chun-Wang Ma. The first draft of the manuscript was written by Kun-Hao Li and all authors commented on previous versions of the manuscript. All authors read and approved the final manuscript.

Data availability The data that support the findings of this study are openly available in Science Data Bank at https://cstr.cn/31253.11.sciencedb.35097 and https://doi.org/10.57760/sciencedb.35097.

Declarations

Conflict of interest Chun-Wang Ma is an editorial board member for Nuclear Science and Techniques and was not involved in the editorial review, or the decision to publish this article. All authors declare that there are no conflict of interest.

References

1. I. Tanihata, H. Savajols, R. Kanungo, Recent experimental progress in nuclear halo structure studies. Prog. Part. Nucl. Phys. **68**, 215–313 (2013). https://doi.org/10.1016/j.ppnp.2012.07.001
2. E. Lunderberg, P.A. DeYoung, Z. Kohley et al., Evidence for the ground-state resonance of ^{26}O. Phys. Rev. Lett. **108**, 142503 (2012). https://doi.org/10.1103/PhysRevLett.108.142503
3. A.H. Wuosmaa, J.P. Schiffer, K.E. Rehm et al., Structure of ^{7}He by proton removal from ^{8}Li with the (d,^{3}He) reaction. Phys. Rev. C **78**, 041302 (2008). https://doi.org/10.1103/PhysRevC.78.041302
4. M.T. Wan, L. Ou, M. Liu et al., Properties of the drip-line nucleus and mass relation of mirror nuclei. Nucl. Sci. Tech. **36**, 26 (2025). https://doi.org/10.1007/s41365-024-01633-9
5. L. Zhou, S.M. Wang, D.Q. Fang et al., Recent progress in two-proton radioactivity. Nucl. Sci. Tech. **33**, 105 (2022). https://doi.org/10.1007/s41365-022-01091-1
6. R.G. Thomas, An analysis of the energy levels of the mirror nuclei, ^{13}C and ^{13}N. Phys. Rev. **88**, 1109–1125 (1952). https://doi.org/10.1103/PhysRev.88.1109
7. J.B. Ehrman, On the displacement of corresponding energy levels of ^{13}C and ^{13}N. Phys. Rev. **81**, 412–416 (1951). https://doi.org/10.1103/PhysRev.81.412
8. K.A. Chipps, D.W. Bardayan, J.C. Blackmon et al., First direct measurement of the ^{17}F$(p,\gamma)^{18}$Ne cross section. Phys. Rev. Lett. **102**, 152502 (2009). https://doi.org/10.1103/PhysRevLett.102.152502
9. J. Lee, X.X. Xu, K. Kaneko et al., Large isospin asymmetry in ^{22}Si/^{22}O mirror Gamow–Teller transitions reveals the halo structure of ^{22}Al. Phys. Rev. Lett. **125**, 192503 (2020). https://doi.org/10.1103/PhysRevLett.125.192503
10. M.Z. Sun, Y. Yu, X.P. Wang et al., Ground-state mass of ^{22}Al and test of state-of-the-art ab initio calculations. Chin. Phys. C **48**, 034002 (2024). https://doi.org/10.1088/1674-1137/ad1a0a
11. H.H. Li, Q. Yuan, J.G. Li et al., Investigation of isospin-symmetry breaking in mirror energy difference and nuclear mass with ab initio calculations. Phys. Rev. C **107**, 014302 (2023). https://doi.org/10.1103/PhysRevC.107.014302
12. C.X. Yuan, C. Qi, F.R. Xu et al., Mirror energy difference and the structure of loosely bound proton-rich nuclei around $A = 20$. Phys. Rev. C **89**, 044327 (2014). https://doi.org/10.1103/PhysRevC.89.044327
13. I. Stefan, F. de Oliveira Santos, O. Sorlin et al., Probing nuclear forces beyond the drip line using the mirror nuclei ^{16}N and ^{16}F. Phys. Rev. C **90**, 014307 (2014). https://doi.org/10.1103/PhysRevC.90.014307
14. J.G. Li, N. Michel, H.H. Li et al., One-neutron halo structure of ^{29}Ne. Phys. Lett. B **832**, 137225 (2022). https://doi.org/10.1016/j.physletb.2022.137225
15. X. Mao, J. Rotureau, W. Nazarewicz et al., Gamow-shell-model description of Li isotopes and their mirror partners. Phys. Rev. C **102**, 024309 (2020). https://doi.org/10.1103/PhysRevC.102.024309
16. N. Michel, J.G. Li, L.H. Ru et al., Calculation of the Thomas–Ehrman shift in ^{16}F and ^{15}O(p,p) cross sections within the Gamow shell model. Phys. Rev. C **106**, L011301 (2022). https://doi.org/10.1103/PhysRevC.106.L011301
17. K. Way, Elementary theory of nuclear shell structure. Science **122**, 603 (1955). https://doi.org/10.1126/science.122.3170.603.b
18. E. Caurier, G. Martínez-Pinedo, F. Nowacki et al., The shell model as a unified view of nuclear structure. Rev. Mod. Phys. **77**, 427–488 (2005). https://doi.org/10.1103/RevModPhys.77.427
19. F. Ajzenberg-Selove, Energy levels of light nuclei $A = 5$–10. Nucl. Phys. A **490**, 1–225 (1988). https://doi.org/10.1016/0375-9474(88)90124-8
20. P. Campbell, I.D. Moore, M.R. Pearson, Laser spectroscopy for nuclear structure physics. Prog. Part. Nucl. Phys. **86**, 127–180 (2016). https://doi.org/10.1016/j.ppnp.2015.09.003
21. J.G. Li, B.S. Hu, S. Zhang et al., Unbound ^{28}O, the heaviest oxygen isotope observed: a cutting-edge probe for testing nuclear models. Nucl. Sci. Tech. **35**, 21 (2024). https://doi.org/10.1007/s41365-024-01373-w
22. C. Angulo, G. Tabacaru, M. Couder et al., Identification of a new low-lying state in the proton drip line nucleus ^{19}Na. Phys. Rev. C **67**, 014308 (2003). https://doi.org/10.1103/PhysRevC.67.014308
23. S. Zhang, Y.Z. Ma, J.G. Li et al., The roles of three-nucleon force and continuum coupling in mirror-symmetry breaking of the oxygen mass region. Phys. Lett. B **827**, 136958 (2022). https://doi.org/10.1016/j.physletb.2022.136958
24. M.A. Bentley, S.M. Lenzi, Coulomb energy differences between high-spin states in isobaric multiplets. Prog. Part. Nucl. Phys. **59**, 497–561 (2007). https://doi.org/10.1016/j.ppnp.2006.10.001
25. A.P. Zuker, S.M. Lenzi, G. Martínez-Pinedo et al., Isobaric multiplet yrast energies and isospin nonconserving forces. Phys. Rev. Lett. **89**, 142502 (2002). https://doi.org/10.1103/PhysRevLett.89.142502
26. K. Kaneko, Y. Sun, T. Mizusaki et al., Variation in displacement energies due to isospin-nonconserving forces. Phys. Rev. Lett. **110**, 172505 (2013). https://doi.org/10.1103/PhysRevLett.110.172505
27. Y.H. Lam, N.A. Smirnova, E. Caurier, Isospin nonconservation in *sd*-shell nuclei. Phys. Rev. C **87**, 054304 (2013). https://doi.org/10.1103/PhysRevC.87.054304
28. A. Magilligan, B.A. Brown, New isospin-breaking USD Hamiltonians for the *sd* shell. Phys. Rev. C **101**, 064312 (2020). https://doi.org/10.1103/PhysRevC.101.064312
29. P. Bączyk, J. Dobaczewski, M. Konieczka, *et al.*, Isospin-symmetry breaking in masses of $N \simeq Z$ nuclei. Phys. Lett. B **778**, 178–183 (2018) https://doi.org/10.1016/j.physletb.2017.12.068
30. R.D.O. Llewellyn, M.A. Bentley, R. Wadsworth et al., Establishing the maximum collectivity in highly deformed $N = Z$ nuclei. Phys. Rev. Lett. **124**, 152501 (2020). https://doi.org/10.1103/PhysRevLett.124.152501
31. J.G. Li, N. Michel, W. Zuo et al., Resonances of $A = 4$, $T = 1$ isospin triplet states within the ab initio no-core Gamow shell model. Phys. Rev. C **104**, 024319 (2021). https://doi.org/10.1103/PhysRevC.104.024319
32. M.S. Martin, S.R. Stroberg, J.D. Holt et al., Testing isospin symmetry breaking in ab initio nuclear theory. Phys. Rev. C **104**, 014324 (2021). https://doi.org/10.1103/PhysRevC.104.014324
33. E. Caurier, P. Navrátil, W.E. Ormand et al., Ab initio shell model for $A = 10$ nuclei. Phys. Rev. C **66**, 024314 (2002). https://doi.org/10.1103/PhysRevC.66.024314
34. J.G. Li, H.H. Li, S. Zhang et al., Double-magicity of proton drip-line nucleus ^{22}Si with ab initio calculation. Phys. Lett. B **846**, 138197 (2023). https://doi.org/10.1016/j.physletb.2023.138197
35. S. Uthayakumaar, M.A. Bentley, E.C. Simpson et al., Spectroscopy of the $T = \frac{3}{2}A = 47$ and $A = 45$ mirror nuclei via one- and two-nucleon knockout reactions. Phys. Rev. C **106**, 024327 (2022). https://doi.org/10.1103/PhysRevC.106.024327
36. H.H. Li, J.G. Li, M.R. Xie et al., Ab initio calculations of mirror energy difference in *sd*-shell nuclei. Chin. Phys. C **47**, 124101 (2023). https://doi.org/10.1088/1674-1137/acf035
37. R. Id-Betan, R.J. Liotta, N. Sandulescu et al., Two-particle resonant states in a many-body mean field. Phys. Rev. Lett. **89**, 042501 (2002). https://doi.org/10.1103/PhysRevLett.89.042501

38. N. Michel, W. Nazarewicz, M. Płoszajczak et al., Gamow shell model description of neutron-rich nuclei. Phys. Rev. Lett. **89**, 042502 (2002). https://doi.org/10.1103/PhysRevLett.89.042502
39. N. Michel, W. Nazarewicz, M. Płoszajczak et al., Shell model in the complex energy plane. J. Phys. G: Nucl. Part. Phys. **36**, 013101 (2009). https://doi.org/10.1088/0954-3899/36/1/013101
40. N. Michel, M. Płoszajczak, in *Gamow Shell Model, The Unified Theory of Nuclear Structure and Reactions* (Springer, Berlin, 2021), pp. 1–514. https://doi.org/10.1007/978-3-030-69356-5
41. J.G. Li, B.S. Hu, Q. Wu et al., Neutron-rich calcium isotopes within realistic Gamow shell model calculations with continuum coupling. Phys. Rev. C **102**, 034302 (2020). https://doi.org/10.1103/PhysRevC.102.034302
42. H.H. Li, J.G. Li, N. Michel et al., Investigation of unbound hydrogen isotopes with the Gamow shell model. Phys. Rev. C **104**, L061306 (2021). https://doi.org/10.1103/PhysRevC.104.L061306
43. J.G. Li, Y.Z. Ma, N. Michel et al., Recent progress in Gamow shell model calculations of drip line nuclei. Physics **3**, 977–997 (2021). https://doi.org/10.3390/physics3040062
44. J.G. Li, N. Michel, W. Zuo et al., Unbound spectra of neutron-rich oxygen isotopes predicted by the Gamow shell model. Phys. Rev. C **103**, 034305 (2021). https://doi.org/10.1103/PhysRevC.103.034305
45. S. Zhang, F.R. Xu, J.G. Li et al., Ab initio descriptions of $A = 16$ mirror nuclei with resonance and continuum coupling. Phys. Rev. C **108**, 064316 (2023). https://doi.org/10.1103/PhysRevC.108.064316
46. T. Berggren, On the use of resonant states in eigenfunction expansions of scattering and reaction amplitudes. Nucl. Phys. A **109**, 265–287 (1968). https://doi.org/10.1016/0375-9474(68)90593-9
47. N. Michel, H.M. Aktulga, Y. Jaganathen, Toward scalable many-body calculations for nuclear open quantum systems using the Gamow shell model. Comput. Phys. Commun. **247**, 106978 (2020). https://doi.org/10.1016/j.cpc.2019.106978
48. Y. Suzuki, K. Ikeda, Cluster-orbital shell model and its application to the He isotopes. Phys. Rev. C **38**, 410–413 (1988). https://doi.org/10.1103/PhysRevC.38.410
49. G. Papadimitriou, A.T. Kruppa, N. Michel et al., Charge radii and neutron correlations in helium halo nuclei. Phys. Rev. C **84**, 051304(R) (2011). https://doi.org/10.1103/PhysRevC.84.051304
50. Y. Jaganathen, R.M. Id-Betan, N. Michel et al., Quantified Gamow shell model interaction for *psd*-shell nuclei. Phys. Rev. C **96**, 054316 (2017). https://doi.org/10.1103/PhysRevC.96.054316
51. H.W. Hammer, A. Nogga, A. Schwenk, Colloquium: three-body forces: from cold atoms to nuclei. Rev. Mod. Phys. **85**, 197–217 (2013). https://doi.org/10.1103/RevModPhys.85.197
52. H.W. Hammer, S. König, U. van Kolck, Nuclear effective field theory: status and perspectives. Rev. Mod. Phys. **92**, 025004 (2020). https://doi.org/10.1103/RevModPhys.92.025004
53. S. Binder, A. Ekström, G. Hagen et al., Effective field theory in the harmonic oscillator basis. Phys. Rev. C **93**, 044332 (2016). https://doi.org/10.1103/PhysRevC.93.044332
54. R.J. Furnstahl, G. Hagen, T. Papenbrock, Corrections to nuclear energies and radii in finite oscillator spaces. Phys. Rev. C **86**, 031301(R) (2012). https://doi.org/10.1103/PhysRevC.86.031301
55. A. Bansal, S. Binder, A. Ekström et al., Pion-less effective field theory for atomic nuclei and lattice nuclei. Phys. Rev. C **98**, 054301 (2018). https://doi.org/10.1103/PhysRevC.98.054301
56. L. Huth, V. Durant, J. Simonis et al., Shell-model interactions from chiral effective field theory. Phys. Rev. C **98**, 044301 (2018). https://doi.org/10.1103/PhysRevC.98.044301
57. N. Michel, J.G. Li, F.R. Xu et al., Description of proton-rich nuclei in the $A \approx 20$ region within the Gamow shell model. Phys. Rev. C **100**, 064303 (2019). https://doi.org/10.1103/PhysRevC.100.064303
58. http://www.nndc.bnl.gov/ensdf
59. M.R. Xie, J.G. Li, N. Michel et al., Investigation of spectroscopic factors of deeply-bound nucleons in drip-line nuclei with the Gamow shell model. Phys. Lett. B **839**, 137800 (2023). https://doi.org/10.1016/j.physletb.2023.137800
60. M.R. Xie, J.G. Li, N. Michel et al., Spectroscopic factors of resonance states with the Gamow shell model. Sci. China Phys. Mech. Astron. **67**, 212011 (2024). https://doi.org/10.1007/s11433-023-2227-5
61. N. Michel, J.G. Li, F.R. Xu et al., Two-neutron halo structure of ^{31}F. Phys. Rev. C **101**, 031301(R) (2020). https://doi.org/10.1103/PhysRevC.101.031301
62. K.H. Li, N. Chen, J.G. Li et al., Gamow shell model calculations for the Thomas–Ehrman shift in the new isotope ^{21}Al. Phys. Rev. C **111**, 034327 (2025). https://doi.org/10.1103/PhysRevC.111.034327
63. Y.M. Xing, Y.F. Luo, Y.H. Zhang et al., $Z = 14$ magicity revealed by the mass of the proton dripline nucleus ^{22}Si. Phys. Rev. Lett. **135**, 012501 (2025). https://doi.org/10.1103/ffwt-n7yc